Detailed kinetic study of anisole pyrolysis and oxidation to understand tar formation during biomass combustion and gasification

Milena Nowakowska, Olivier Herbinet, Anthony Dufour, Pierre-Alexandre Glaude

Detailed kinetic study of anisole pyrolysis and oxidation to understand tar formation during biomass combustion and gasification

Milena Nowakowska, Olivier Herbinet, Anthony Dufour, Pierre-Alexandre Glaude*

Laboratoire Réactions et Génie des Procédés (LRGP), CNRS, Université de Lorraine, ENSIC, 1 rue Grandville, 54000 Nancy, France

Abstract

Anisole was chosen as the simplest surrogate for primary tar from lignin pyrolysis to study the gas-phase chemistry of methoxyphenol conversion. Methoxyphenols are one of the main precursors of PAH and soot in biomass combustion and gasification. These reactions are of paramount importance for the atmospheric environment, to mitigate emissions from wood combustion, and for reducing tar formation during gasification. Anisole pyrolysis and stoichiometric oxidation were studied in a jet-stirred reactor (673–1173 K, residence time 2 s, 800 Torr (106.7 kPa), under dilute conditions) coupled with gas chromatography–flame ionization detector and mass spectrometry. Decomposition of anisole starts at 750 K and a conversion degree of 50% is obtained at about 850 K under both studied conditions. The main products of reaction vary with temperature and are phenol, methane, carbon monoxide, benzene, and hydrogen. A detailed kinetic model (303 species, 1922 reactions) based on a combustion model for light aromatic compounds has been extended to anisole. The model predicts the conversion of anisole and the formation of the main products well. The reaction flux analyses show that anisole decomposes mainly to phenoxy and methyl radicals in both pyrolysis and oxidation conditions. The decomposition of phenoxy radicals is the main source of cyclopentadienyl radicals, which are the main precursor of naphthalene and heavier PAH in these conditions.

Keywords: Anisole; Pyrolysis; Oxidation; Tars; Biomass; Kinetic modeling

Corresponding author: pierre-alexandre.glaude@univ-lorraine.fr

1. Introduction

Environmental concerns such as the control of greenhouse gas emissions have led to an increased interest in the use of renewable energy. Biomass is widely used in combustion but can also be utilized in more advanced applications such as the production of a synthesis gas (syngas, a mixture of CO and H_2), which can be used for the production of liquid fuels such as Fisher–Tropsch or methanol. Lignocellulosic biomass may be a promising feedstock through the gasification processes [1] and [2], but tar is also formed during gasification [3]. The tar content in the product gas is the major cumbersome and problematic parameter in the gasification processes [4]. Tar represents a complex mixture of over 100 compounds [5] and [6]. It leads to fouling, coke deposition, and catalyst deactivation. Hence, tar conversion or removal is one of the main challenges for the successful development of commercial gasification technologies and has been extensively studied [7] and [8].

Evans and Milne [5] defined three main classes of tars: primary tars (low temperature, oxygenated) and secondary and tertiary tars (benzene, polycyclic aromatic hydrocarbons—PAHs, etc.). In combustion and gasification reactors, the heaviest (tertiary) tars are formed by the conversion of primary tars, for instance, in the freeboard or emulsion phase of a fluidized bed or in the flame during combustion. A better understanding of the detailed gas-phase chemistry leading from primary tars to secondary and tertiary ones is needed. The aim of this work is to deeply understand these reactions under conditions representative of biomass gasification in air-blown fluidized beds, but also PAH formation in wood combustion furnaces [9]. A significant fraction of aromatic tars and soot originates from lignin pyrolysis products mainly composed of guaiacol-type and syringol-type units [5], [10], [11] and [12]. Carbohydrates from cellulose and hemicellulose can also contribute to aromatic formation through the production of light unsaturated species such as acetylene and propargyl radicals [5], [13] and [14]. The simplest aromatic model compound with a methyl ether unit, which is anisole, has been chosen as a surrogate for lignin primary tar, as a first step toward developing an advanced elementary kinetic model including major primary tar surrogates.

To date, there have been very few works on tar gas-phase conversion coupling well-controlled experiments, tar quantitative analysis, and elementary modeling, especially concerning anisole. Earlier experiments for anisole pyrolysis were performed in a stirred-flow reactor by Mulcahy et al. [15], who reported that reactions between methyl radicals and anisole proceed mainly by H-abstraction on the methoxy group, which is about 12 times faster than the attack on the aromatic ring. A mechanism for the formation of the main identified products (benzaldehyde, toluene, and methane) was also proposed. During the 1980s, Schlosberg et al. [16] quantified 10 products of anisole decomposition after a 2-min pyrolysis at 723 K. A shock tube study of the decomposition of anisole between 1000 and 1580 K and at pressures from 0.4 to 0.9 atm permitted an evaluation of the rate constant of the unimolecular decomposition of phenoxy radicals (C_6H_5O) to CO and C_5H_5 and of the reaction of methyl radicals with phenoxy to form cresols [17]. Mackie et al. [18] studied the pyrolysis of anisole in a perfectly stirred reactor over the temperature range 850–1000 K and at low pressure (between 16 and 120 × 10^{-3} atm). The yields of the main products (CH_4, C_2H_6, C_6H_5OH, methylcyclopentadiene, CO, cresols, benzene, and benzaldehyde) as functions of temperature at two residence times (0.14 and 0.95 s) were reported and a rate constant was proposed for the unimolecular decomposition of anisole:

$$C_6H_5OCH_3 \rightarrow C_6H_5O + CH_3$$

Rate parameters were A = (2.9 ± 1.0) × 10^{15} s^{-1} and Ea = 64.0 ± 0.6 kcal/mol. Arends et al. [19] studied the thermal decomposition of anisole in an excess of hydrogen in a flow reactor over the temperature range 793–1020 K and at atmospheric pressure. The main identified products were similar to those found in previous studies. A first kinetic model for anisole decomposition was proposed, which was composed of 37 reactions involving 23 species. However, some assumptions on

the rate constant were made to obtain good agreement with experimental results. Pecullan et al. [20] presented the first study on anisole oxidation. Experiments near 1000 K were performed in the Princeton flow reactor and made it possible to observe that anisole undergoes first-order decay under both pyrolysis and oxidation conditions. It was proved also that under the studied conditions, the distribution of reaction products such as phenol, cresols, methane, and ethane was independent of the equivalence ratio. A new kinetic model was proposed, consisting of 66 reversible reactions involving 31 species. A good prediction of experimental data was reached for anisole, carbon monoxide, methylcyclopentadiene, and total phenolic compounds. More recently, Platonov et al. [21] showed the formation of various decomposition products, including PAHs, during the pyrolysis of anisole at high temperature (1023–1173 K). Friderichsen et al. [22] used a hyperthermal nozzle and a flow tube reactor followed by analysis by mass spectrometry and FTIR spectroscopy. Phenoxy and cyclopentadienyl radicals were found to be important intermediates in the decomposition of anisole. In addition, the identification of 9,10-dihydrofulvalene suggested that this molecule can be considered as a naphthalene precursor (2 C_5H_5 → 9,10-dihydrofulvalene → naphthalene). To observe radical intermediates, Scheer et al. [23] and [24] used a hyperthermal tubular flow reactor with about 65 µs residence time. Their results confirm that the first step in the decomposition of anisole is the loss of the methyl group to form a phenoxy radical, followed by the ejection of CO to yield a cyclopentadienyl radical. They showed also that C5H5 decomposes to the propargyl radical (CH_2CCH) and acetylene only at high temperature (>1373 K). Afterward, propargyl radical recombination is a significant benzene formation channel. At lower temperatures, most of benzene comes from a ring expansion reaction of methylcyclopentadiene (MCPD), resulting from methyl radicals combining with cyclopentadienyl radicals. Naphthalene formation was attributed also to cyclopentadienyl radical combination. The most recent paper dealing with anisole [25] proposed a new kinetic mechanism validated against experimental data from Pecullan et al. [20] and Platonov et al. [21]. The literature review shows that anisole is a fragile compound, which reacts easily by unimolecular O-CH_3 bond breaking, which leads to methyl and phenoxy radicals. This is consistent with the bond dissociation energies [26] and [27] involved in anisole and presented in Figure 1.

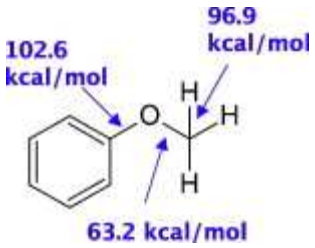

Figure 1: Structure of anisole and bond dissociation energies.

To the best of our knowledge and despite all these extensive works, there is not yet a detailed kinetic mechanism for anisole pyrolysis and oxidation validated against well-controlled thermal conditions with quantitative analysis of products. Moreover, while the very low value of the C-O bond dissociation energy allows easy decomposition, most studies have been performed at temperatures higher than 1000 K, i.e., higher than that involved in biomass pyrolysis/gasification where primary tars are formed. The present work aims at investigating experimentally and theoretically the kinetics of anisole pyrolysis and oxidation at intermediate temperatures (673–1173 K) and to predict the formation of intermediates leading to secondary and tertiary tars, such as PAHs.

2. Experimental methods

The experimental study was performed in a jet-stirred reactor operated at constant temperature and pressure. The experimental apparatus has already been used for numerous pyrolysis and oxidation gas phase studies. Its description can be found in previous papers [28] and [29]. The main features of the experimental and analytical methods are described below. It has been shown that under the

present conditions, this reactor can be considered as a zero-dimensional ideal perfectly stirred reactor with homogenous temperature and composition. The jet-stirred reactor (Figure 2) is made of fused silica and consists of an annular preheater and of a sphere in which the reaction takes place, with an injection cross located at the center. The reactor (volume 88 cm^3) and the injection cross were designed to obtain four turbulent jets, providing good mixing of the gas phase [30]. The heating of the preheater and of the reactor is achieved by the mean of Thermocoax resistances rolled around the different parts and controlled by Eurotherm 3216 controllers and type K thermocouples (temperature precision better than 1%). The heating of the preheater is divided into two zones, the first one heated at a temperature 150 K lower than the reaction temperature and the second one being heated at the same temperature as the reactor. The reaction temperature was measured by another type K thermocouple located in the intra-annular part of the preheater, with its extremity at the level of the injection cross in the center of the reactor.

Figure 2: Jet-stirred reactor (JSR) used to study the gas-phase conversion of anisole.

The feed of liquid anisole (Sigma Aldrich, purity 99.7%) was controlled by a Coriolis mass flow controller (Bronkhorst). This device was associated with an evaporator in which anisole was mixed with the carrier gas (helium IC or argon 5.0, Messer) and heated to 473 K. The carrier gas flow rate was controlled by a gas mass flow controller (Bronkhorst). The precision of the mass flow controllers is 0.5%. The carrier gas for experiments was helium. A set of experiments was also performed with argon to enable the quantification of hydrogen. The pressure in the reactor was kept constant at 800 Torr (106.7 kPa) using a valve located downstream of the reactor. The residence time of anisole was 2 s for both pyrolysis and oxidation studies.

Unconverted reactant and products were analyzed by means of several gas chromatographs (GC). For pyrolysis studies, the analysis was performed in two steps, as light and heavy species could not be analyzed at the same time. Heavy species (including more than five heavy atoms such as carbon and oxygen) were condensed in a trap connected to the reactor outlet and maintained at liquid nitrogen temperature. The content of the trap after addition of an internal standard (n-octane) and solvent (acetone) was analyzed in an Agilent 7890. A gas chromatograph fitted with an HP-5 capillary column, a flame ionization detector (FID), and a mass spectrometer for species identification. Light species (including less than six heavy atoms) were analyzed online using two gas chromatographs. The first one was fitted with a Plot-Q capillary column (providing good separation for hydrocarbons from methane to 1,3-cyclopentadiene) and a FID; the second one with a Carbosphere packed column (providing good separation for methane, C_2 hydrocarbons, and carbon oxides), a thermal conductivity detector (TCD), and a FID. Hydrogen was quantified using a Perichrome 1250 gas chromatograph fitted with a 5-Å molecular sieve and a TCD. The carrier gas in the JSR was switched from helium to argon for these analyses to enhance the sensitivity and to avoid the superposition of a peak of helium with the peak of H_2. In the case of oxidation studies, the whole analysis was made online with a transfer line to GC heated to 413 K to avoid the condensation of heavy products. It has been checked that both methods (on-line and off-line) led to similar results. Note also that in the

temperature range used in this study, the amount of radical species remains low in comparison with that of stable products; combination reactions cannot really affect the quantification. All the products were analyzed by gas chromatography using the instruments mentioned before. For heavy products, the calibration was made using a gas sample of known composition for anisole, benzene, toluene, phenol, and cresols. In the case of other heavy products, the carbon effective number method [31] was applied to quantify other species with anisole as a reference. The limit of detection was about 1 ppm for the heaviest species (FID), about 10 ppm for carbon oxides and oxygen (TCD), and 100 ppm for hydrogen. Uncertainty estimates were about ±5% for species that are analyzed online and ±10% for species condensed in the trap in pyrolysis experiments. In the case of phenolic compounds, i.e., phenol and cresols, their high affinity for surfaces led to higher uncertainties, around 30%.

Two series of experiments, in pyrolysis and oxidation respectively, were made in the range of temperature 673–1173 K. Measures were made every 25 K to follow the decay of the reactant mole fraction and also the evolution of the product mole fraction profiles. The inlet mole fraction of anisole was 0.01 in pyrolysis experiments, and was reduced to 0.005 in the oxidation study to avoid the fouling of the heated transfer line to the GCs. Oxidation experiments were performed under stoichiometric conditions (φ = 1). In pyrolysis, the carbon mass balance was better than 95% up to 1100 K. Above this temperature, a progressive decrease in the carbon balance was observed, due to the formation of heavy PAHs and soots, which were not quantified. In oxidation, the mass balance remained correct over the whole temperature range, since carbon oxides are obtained at high temperature.

3. Kinetic modeling

A new detailed kinetic model for the pyrolysis and combustion of anisole has been developed based on a recent model of ethylbenzene oxidation [32], which was used as a comprehensive reaction base for the reaction of aromatics and smaller species. This mechanism contains the different reaction pathways producing aromatic rings from lighter species, such as propargyl radical combinations and C4 and cyclopentadienyl reaction routes [33]. A submechanism for the reactions of anisole has been developed in the present work. Reactions of xylenes [34] and the reactions of formation of PAHs proposed by Slavinskaya et al. [35] have been included. Reactions with acetylene, involved in the so-called HACA mechanism, are included. Reactions of benzaldehyde, cresols, and naphthalene have been revised. The final model contains 303 species and 1922 reactions. Simulations were performed using the PSR (perfectly stirrer reactor model) module in the Chemkin software suite [36]. Thermochemical data were mainly evaluated by the software THERGAS [27].

The primary mechanism for anisole decomposition and oxidation is composed of 24 elementary reactions (Table 1) including initiations, ipso-additions, H-abstractions, and radical decompositions. Reactions of initiation include the breaking of the two weakest bonds in the anisole molecule, i.e., O-CH_3 and OCH_2-H bonds. Kinetic parameters of these two channels were estimated from the reverse radical combinations. The breaking of the C-O bond leading to phenoxy and CH_3 radicals (reaction 1 in Table 1) uses the same kinetic parameters for the reverse reaction as that used in the termination of benzyl radicals with CH3, forming ethylbenzene [37]. This corresponds to a value of the first-order decomposition of anisole at the upper limit in the uncertainty range of the rate constant proposed by Mackie et al. [18], with a factor of 2.2 at 1000 K. The breaking of the C-H bond (reaction 2) is modeled by kinetic parameters estimated by analogy with alkyl radicals [38]. Bimolecular initiations with oxygen molecules produce View the $C_6H_5OCH_2\bullet$ and HO_2 radicals (reaction 3). Kinetic parameters were estimated using rules proposed by Ingham and Walker for the alkanes [39], assuming an activation energy equal to the enthalpy of reaction. Ipso-additions involving H-atom, OH, and CH_3 radicals have been considered. For the reaction of anisole with H (reaction 4), the kinetic parameters of the equivalent reaction phenol + H were used [37]. Parameters for the reaction with

OH (reaction 5) were estimated by analogy with the similar reaction of toluene + OH [40]. In the case of the reaction with CH3 (reaction 6), kinetic parameters were assumed to be that of the addition of a CH3 radical on a C=C bond [41]. Nine hydrogen atom abstractions on the methoxy group of anisole were also considered. Abstractions by H, OH, and HO_2 (reaction 8–10) were estimated using an Evans–Polanyi relationship proposed by Dean and Bozzelli for the reactions of alkanes [42]. In the case of abstraction by H-atoms (reaction 8), this correlation leads to a high rate constant for the C-H bonds of weak bond dissociation energy [43].

Table 1: Primary mechanism for anisole pyrolysis and oxidation.

Reaction	*A*	*n*	E_a
Initiations			
(1) $C_6H_5O + CH_3$ = anisole	5.0E12	0	0
(2) $C_6H_5OCH_2 + H$ = anisole	1.0E14	0	0
Bimolecular initiation			
(3) Anisole + O_2 = $C_6H_5OCH_2 + OOH$	2.1E13	0	47,900
Ipso-additions			
(4) Anisole + H = $C_6H_6 + CH_3O$	2.23E13	0	7930
(5) Anisole + OH = $C_6H_5OH + CH_3O$	7.8E2	2.88	3220
(6) Anisole + CH_3 = toluene + CH_3O	9.64E10	0.0	8000
H-abstractions			
(7) O + anisole = $OH + C_6H_5OCH_2$	3.0E13	0.0	3280
(8) Anisole + H = $H_2 + C_6H_5OCH_2$	3.6E8	1.5	5730
(9) Anisole + OH = $H_2O + C_6H_5OCH_2$	3.6E6	2.0	−850
(10) Anisole + OOH = $H_2O_2 + C_6H_5OCH_2$	4.2E3	2.69	16,590
(11) Anisole + CH_3 = $CH_4 + C_6H_5OCH_2$	5.01E11	0.0	10,500
(12) Anisole + C_2H_5 = $C_2H_6 + C_6H_5OCH_2$	3.0E11	0.0	9200
(13) Anisole + C_5H_5 = $C_5H_6 + C_6H_5OCH_2$	5.40	3.3	17,200
(14) Anisole + C_6H_5 = $C_6H_6 + C_6H_5OCH_2$	3E11	0.0	3850
(15) $C_6H_5OH + C_6H_5OCH_2$ = anisole + C_6H_5O	1.8E11	0.0	7700
Radical decompositions			
(16) $C_6H_5OCH_2$ = HCHO + C_6H_5	2.61E14	0.05	39,280
(17) $C_6H_5OCH_2$ = $C_6H_5CH_2O$	8.78E10	0.44	19,030
(18) $C_6H_5CH_2O$ = C_6H_5CHO + H	5.26E28	−5.08	22,250
(19) $C_6H_5CH_2O$ = C_6H_6 + CHO	2.37E32	−6.09	28,810
(20) $C_6H_5CH_2O$ = C_6H_5 + HCHO	7.21E33	−6.21	36,850
(21) $C_6H_5CH_2O + H$ = $C_6H_5CH_2OH$	1.0E14	0.0	0.0
(22) $C_6H_5CH_2O + CH_3$ = $C_6H_5CHO + CH_4$	1.0E12	0.0	0.0
(23) $C_6H_5CH_2O + H$ = $C_6H_5CHO + H_2$	1.0E13	0.0	0.0
(24) $C_6H_5CH_2O + C_6H_5$ = $C_6H_5CHO + C_6H_6$	1.0E12	0.0	0.0

Note: Rate constants are given in the form $k = A\,T^n \exp(-E_a/RT)$ where A has units of cm, mol, and s, T has units of K, and E_a has units of cal/mol. The origin of the rate parameters is discussed in the text.

The rate constant was consequently decreased to slow down this reaction, which is very sensitive at the lowest studied temperatures: the A-factor was divided by 2 and the activation energy was increased by 1 kcal/mol, which is in the range of uncertainty of the correlation used. Kinetic parameters for H-abstractions by O atoms and C_2H_5 radicals (reactions 7, 12) were estimated by analogy with the abstraction of a tertiary hydrogen in alkanes [44] because of the similarity between

the bond dissociation energy of both C-H types. Rate parameters for the H-atom abstraction of anisole by the methyl radical CH_3 (reaction 11) were proposed in the literature by Mulcahy et al. [15]. Parameters for the reaction with the cyclopentadienyl radical (reaction 13) were estimated by analogy with the reaction of allyl with *iso*-butane [45], and that with the phenyl radical (reaction 14) by analogy with the reaction of phenyl with propane [46]. The reaction with phenoxy radical (reaction 15) was written in the reverse direction and its rate parameter was estimated from that of the reaction $C_6H_5OH + CH_3 = C_6H_5O + CH_4$ [47]. H-atom abstractions produce $C_6H_5OCH_2\bullet$ radicals, which can react by β-scission (reaction 16) or isomerize to $C_6H_5OCH_2\bullet$ by an internal ipso addition (reaction 17). This latter decomposes afterward, mainly to benzaldehyde (reactions 18–20). Kinetic parameters are those theoretically calculated by da Silva and Bozzelli [48]. The combination of $C_6H_5CH_2O$ with the H-atom (reaction 21) and the disproportionations between $C_6H_5CH_2O$ and the H-atom, CH_3, and C_5H_5 were also added (reactions 22–24), with kinetic parameters estimated by analogy with the same types of reactions in alkane pyrolysis [38].

Some sensitive reactions have been also updated in the model of ethylbenzene oxidation [32] used as a reaction base for the combustion of aromatic compounds. They are summarized in Table 2. Note that this reaction base was validated and used previously for combustion conditions, in which sensitive reactions are different. The modifications were made principally in phenol, 1,3-cyclopentadiene, and benzene submechanisms.

In the phenol submechanism, the high-pressure kinetic parameters for the reaction of combination of phenoxy radicals and hydrogen atoms (reaction 1 in Table 2) have been updated from He et al. [49]. The decomposition of the phenoxy radical to cyclopentadiene and carbon monoxide (reactions 2–3) has been described in more detail. Up to now, the phenoxy radical decomposed directly into C_5H_5 and CO in the mechanisms proposed in the literature. According to theoretical calculations made in our laboratory, and including the pressure dependence [50], a first step has been added in which the phenoxy radical isomerizes to a bicyclic radical; this bicycle further forms a cyclopentadiene radical and carbon monoxide (reaction 3). The rate constant derived from theoretical calculations proposed by Xu and Lin [51] was used for the decomposition of phenol to C_5H_6 and CO (reaction 4) [51]. Reactions of phenoxy radical with CH_3, which especially produce cresols, were added on the basis of the theoretical calculations by Pecullan et al. (reactions 5–8) [20].

The 1,3-cyclopentadiene submechanism was found to be very sensitive in the fate of the phenolic intermediates. For reaction $C_5H_6 = C_5H_5 + H$ (reaction 9), kinetics parameters from Robinson and Lindstedt [52] recommended at 1 atm were used. H-atom abstractions by H-atoms and CH_3 radicals were also reevaluated. The abstraction by H-atoms (reaction 10) was reevaluated theoretically at the CBS-QB3 level of theory [50] and the one involving CH_3 radicals was taken from Pecullan et al. [20] (reaction 11). The addition of H-atom on cyclopentadiene leading to allyl radical and C_2H_2 (reaction 12) was added with the rate constant from Zhong and Bozzelli [53]. H-atom abstractions by C_3H_3 (reaction 14, producing allene or propyne), C_4H_3 (reaction 15, producing vinylacetylene), and C_5H_7 (reaction 16, producing cyclopentene) were added and their rate constants were estimated by analogy with the equivalent H-atom abstractions on toluene [29]. The reaction rate of C_6H_5CO decomposition (reaction 17) was updated from Nam et al. [54] and the kinetic parameters for reaction $C_6H_6 + H = C_5H_4CH_3$ (reaction 18) were taken from Marinov et al. [55]. The H-atom abstraction by C_6H_5 on C_2H_4 to form benzene and C_2H_3 radical (reaction 19) was included based on the data from Tokmakov and Lin [56]. Thermochemical data for phenoxy radicals, cyclopentadienyl radicals, and benzyne were also updated, using data proposed by Sirjean et al. [50], Burcat's database [57], and JetSurf [58], respectively.

Table 2: Modifications in the mechanism of ethylbenzene oxidation [32].

Reaction	A	n	E_a
Phenol submechanism			
(1) $C_6H_5O + H(+M) = C_6H_5OH(+M)$	2.00E14	0	0
(2) C_6H_5O = bicycle	6.17E78	−18.794	90,500
(3) bicycle = $C_5H_5 + CO$	8.29E20	−2.422	11,110
(4) $C_6H_5OH = C_5H_6 + CO$	2.67E14	−0.61	74,100
(5) $C_6H_5O + CH_3$ = MCPD + CO	2.05E+75	−18.29	38,900
(6) $C_6H_5O + CH_3 = OC_6H_4CH_3 + H$	3.33E+39	−7.78	31,700
(7) $C_6H_5O + CH_3 = HOC_6H_4CH_3$	2.31E+73	−17.37	38,800
(8) $C_6H_5O + CH_3 = C_6H_4OH + CH_3$	1.29E−31	13.2	15,600
1,3-Cyclopentadiene submechanism			
(9) $C_5H_6 = C_5H_5 + H$	3.23E49	−10.01	101,130
(10) $C_5H_6 + H = C_5H_5 + H_2$	6.67E07	1.874	4259
(11) $C_5H_6 + CH_3 = C_5H_5 + CH_4$	3.11E11	0	5500
(12) $C_5H_6 + H = C_3H_5 + C_2H_2$	7.74E36	−6.81	32,920
(13) $C_5H_6 + C_3H_3 = C_5H_5 + aC_3H_4$	0.8E12	0	15,100
(14) $C_5H_6 + C_3H_3 = C_5H_5 + pC_3H_4$	0.8E12	0	15,100
(15) $C_5H_6 + C_4H_3 = C_5H_5 + C_4H_4$	1.6E12	0	15,100
(16) $C_5H_6 + C_5H_7 = C_5H_5 + C_5H_8$	1.6E12	0	15,100
Benzene submechanism			
(17) $C_6H_5CO = C_6H_5 + CO$	5.27E14	0	29,010
(18) $C_6H_6 + H = C_5H_5CH_3$	2.39E27	−3.92	29,200
(19) $C_6H_5 + C_2H_4 = C_6H_6 + C_2H_3$	9.45E−3	4.47	4470

Note: Rate constants are given in the form $k = A\,T^n \exp(-E_a/RT)$ where A has units of cm, mol, and s, T has units of K, and E_a has units of cal/mol. The origin of the rate parameters is discussed in the text.

4. Results

4.1. Experimental results

The pyrolysis of anisole has been investigated as a function of the temperature under the conditions described above. The evolution of the mole fraction of anisole is displayed in Figure 3. Anisole starts to decompose at 750 K and reaches 50% conversion at 873 K. Above 950 K, the conversion is complete and the fraction of anisole becomes close to zero. The reaction leads to the formation of dozens of compounds.

Light products include hydrogen, carbon monoxide, methane, ethane, ethylene, and acetylene, profiles of which are presented in Figure 4. These compounds reach high mole fractions and are mostly produced at high temperature. In the case of methane, a shoulder in the mole fraction profile can be seen between 900 and 950 K, which indicates a change in the mechanism. Methane is usually produced by H-atom abstraction by methyl radicals. This transition corresponds to the temperature of complete conversion of anisole. At higher temperature, the reactions of the products of anisole decomposition become dominant in the mixture; H-atom abstractions on these products may be more difficult than on anisole, and other reactions, such as addition on unsaturated bonds, may compete with the methane formation. Among the C_2 species, ethane and ethylene reach a maximum mole fraction about 1000 ppm, around 975 K and 1100 K, respectively. Acetylene is produced in large amounts above 1000 K.

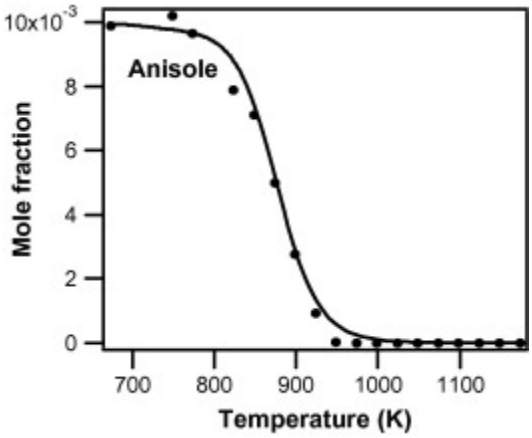

Figure 3: Thermal decomposition of anisole. Points refer to experiments and lines to modeling.

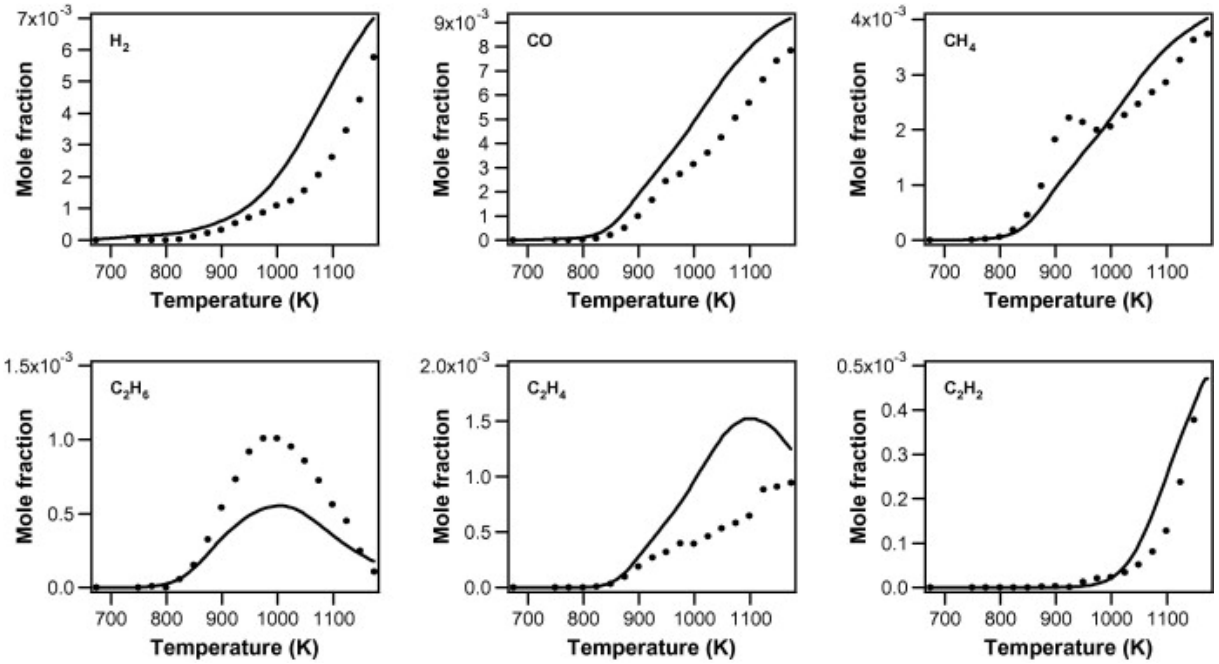

Figure 4: Evolution of the mole fraction of light products of anisole pyrolysis at residence time 2 s and pressure 800 Torr. Points refer to experiments and lines to modeling.

Nonaromatic decomposition products are presented in Figure 5. Propane, propene, propyne, allene, 1,3-butadiene C_4H_6, vinylacetylene C_4H_4, 1,3-cyclopentadiene C_5H_6, and 5-methyl,1,3-cyclopentadiene $CH_3C_5H_5$ have been quantified. In contrast to C_2 species, C_3 and C_4 compounds are produced in small amounts: propene reaches a maximum of 25 ppm, propyne of 21 ppm, while propane, allene, C_4H_6, and C_4H_4 fractions are below 10 ppm. Conversely, 1,3-cyclopentadiene and 5-methyl,1,3-cyclopentadiene mole fractions peak at 400 ppm at 1073 K and 300 ppm at about 950 K, respectively. These observations are consistent with the decomposition channel of anisole to methyl and phenoxy radicals proposed in the literature [18], [19] and [20]. Methyl radicals can react indeed by H-atom abstraction on the reactant to produce methane and by combination to yield ethane and ethylene, leading to large amounts of these molecules. Phenoxy radicals can decompose to CO and cyclopentadienyl radicals. These latter radicals lead to the formation of 1,3-cyclopentadiene and of 5-methyl,1,3-cyclopentadiene by reactions with H-atoms and methyl radicals, respectively.

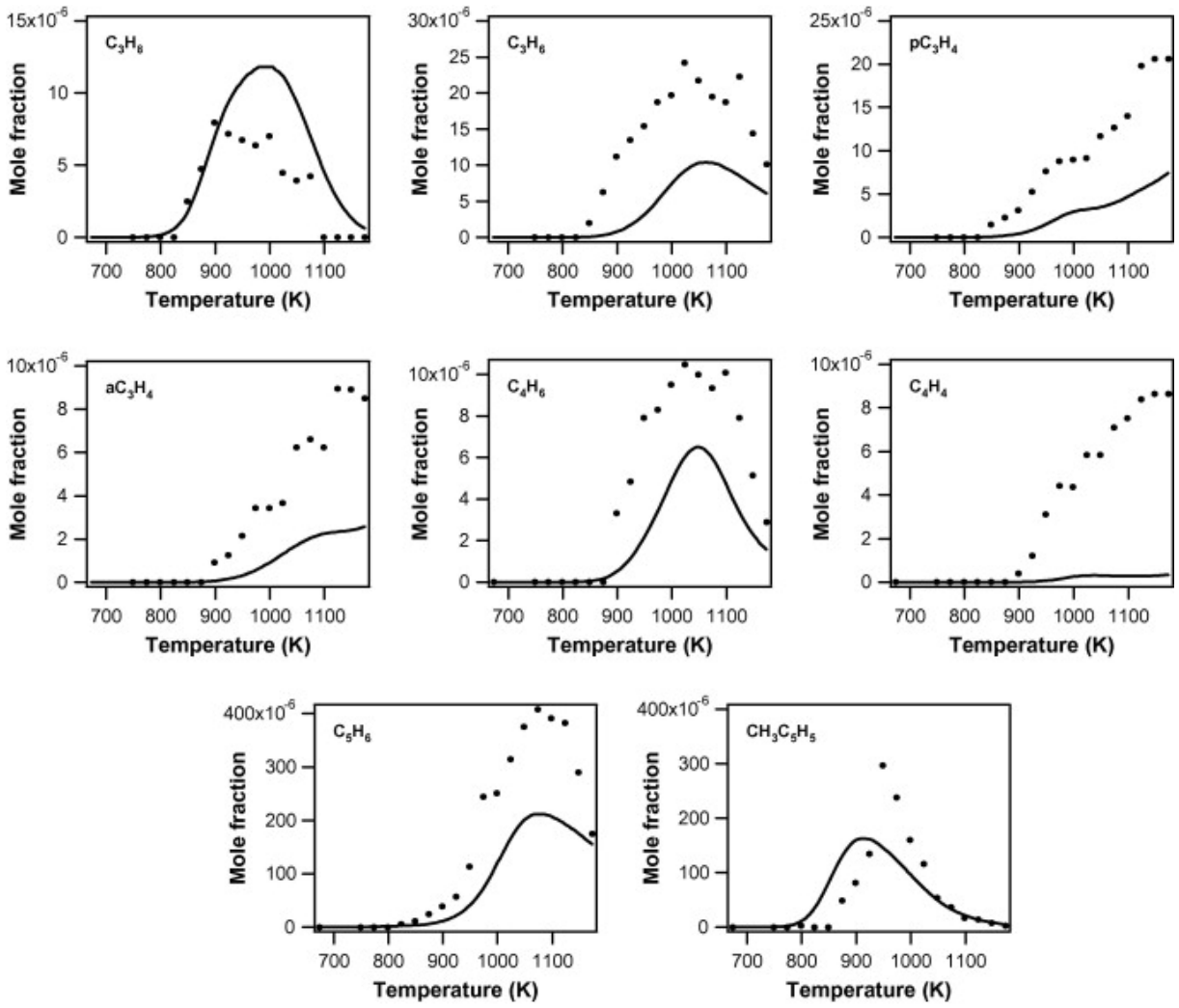

Figure 5: Evolution of the mole fraction of nonaromatic C_3-C_6 products of anisole pyrolysis at residence time 2 s and pressure 800 Torr. Points refer to experiments and lines to modeling.

Aromatic products are displayed in Figure 6. Benzaldehyde, phenol, cresols, and benzofuran, which contain an O-atom like anisole, have been quantified. Benzaldehyde is produced at the lowest temperatures, corresponding to the very beginning of the decomposition reaction of anisole, and its mole fraction reaches a maximum of about 250 ppm at 900 K. Phenol, cresols, and benzofuran are produced in larger amounts, around 5000, 1300, and 750 ppm, respectively. The main aromatic hydrocarbons are benzene, toluene, o- and p-xylene, ethylbenzene, styrene, naphthalene, and acenaphthylene. Benzene is the major one, with a peak around 2700 ppm. Naphthalene is produced at the highest studied temperatures (from 1000 K) and reaches 1000 ppm. The maximum mole fraction of toluene is around 300 ppm, while other products are minor. Note that heavier compounds such as dibenzofuran or phenanthrene were also detected in small amounts but could not be quantified with proper reproducibility. Some soot deposits were obtained at the exit of the reactor at the highest temperatures.

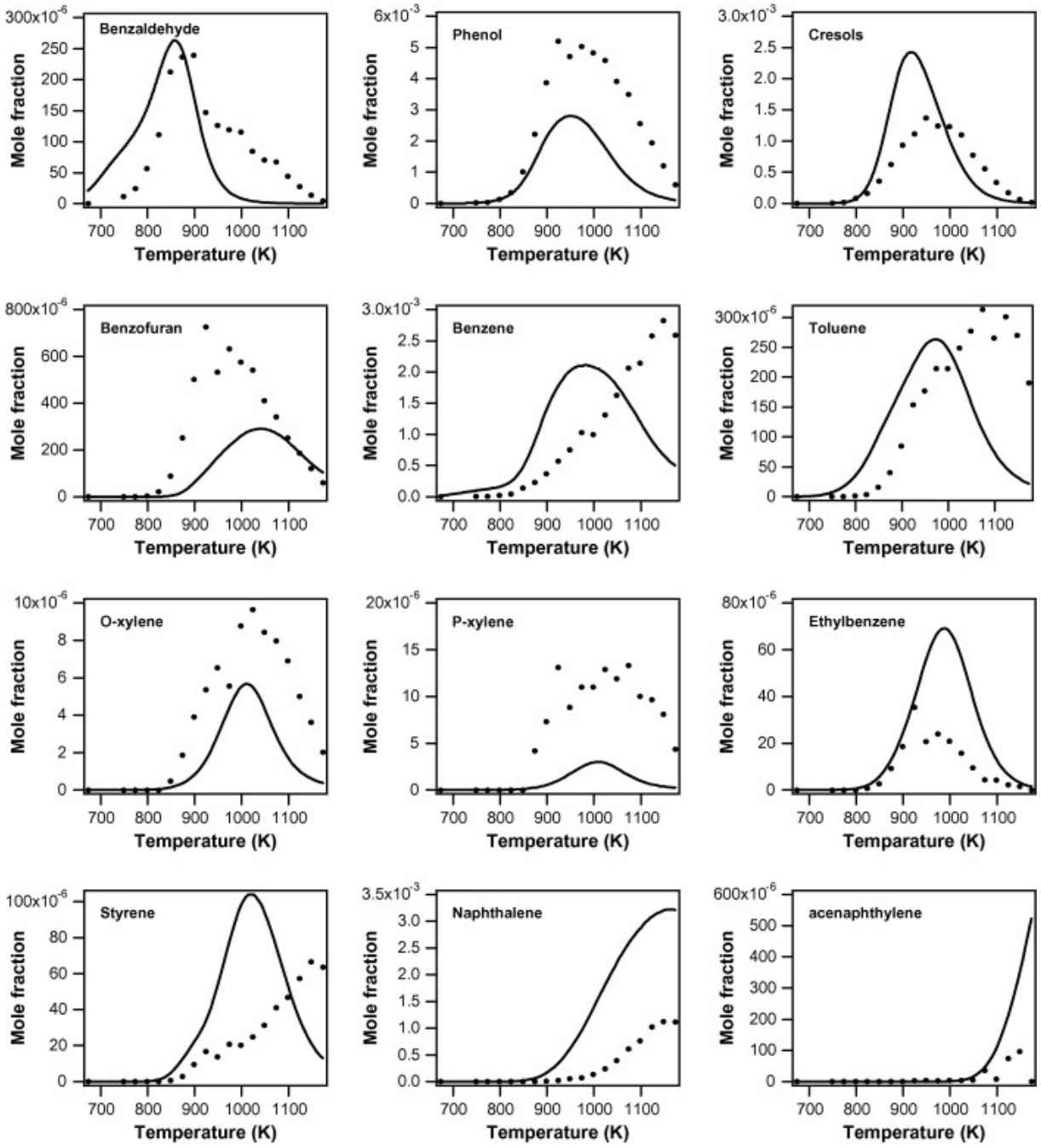

Figure 6: Evolution of the mole fraction of aromatic products of anisole pyrolysis at residence time 2 s and pressure 800 Torr. Points refer to experiments and lines to modeling.

Among the products, two groups can be distinguished: first, compounds with a bell-shaped profile such as phenol or cresols; second, products exhibiting a monotone profile such as CO, hydrogen, or acetylene. The selectivity of the reaction products varies as a function of the temperature. Below 950 K, the main products are phenol, methane, carbon monoxide, cresols, benzaldehyde, and benzofuran. When the temperature increases above 950 K, anisole is completely converted and primary products also reach a high degree of reaction. The major products are then carbon monoxide, hydrogen, methane, benzene, and polyaromatic species. Figure 7 presents the selectivity of anisole and oxygenated products among the oxygenated species as a function of temperature. Phenolic compounds are phenol, o-cresol, and p-cresol; furans are benzofuran and dibenzofuran. Phenolic compounds constitute the major oxygenated compounds below 1050 K. At higher temperatures, CO becomes the major oxygenate formed by the decomposition of the phenol and its

derivatives, which leads also to aromatics, mainly benzene and naphthalene (Figure 6). Note that conversely to usual combustion conditions, light unsaturated soot precursors such as acetylene, allene, and propyne seem to be present in small amounts, which cannot yield noticeable amounts of aromatics. Furthermore, aromatic and polyaromatic hydrocarbon formation starts around 900 K, at temperatures much lower than those typical for such mechanisms [33]. Benzaldehyde exhibits noticeable selectivity only at the lowest temperature, while furans remain minor products over the whole temperature range. This evolution corresponds to the maturation of tars described by Evans and Milne [5], going from primary tars, for which anisole is the simplest surrogate from lignin, to secondary tars, i.e., the phenolic compounds, and to tertiary tars, which are aromatics and polyaromatics produced by the decomposition of the phenolic molecules and the combination of light unsaturated hydrocarbons. The color of the solutions sampled in the condensers (Figure S1 in the Supplementary material) also illustrates this observation by varying significantly with the temperature from transparent (773–823 K) to yellow (873–1023 K) and brown (>1023 K), highlighting the formation of heavy species and even soots.

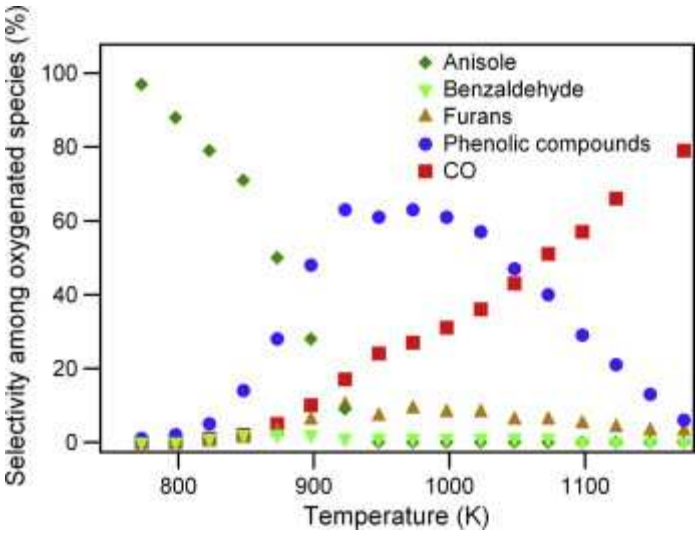

Figure 7: Selectivity of selected compounds among the oxygenated species (mol%) as a function of temperature during the pyrolysis of anisole.

The stoichiometric oxidation of anisole has been also investigated as a function of the temperature under the conditions described above. The evolution of the mole fraction of the reactants is displayed in Figure 8. The temperatures corresponding to the start of the reaction, the consumption of 50% of anisole, and the total conversion of the reactant are exactly the same as obtained in thermal decomposition, which is consistent with observations in the literature [20]. Anisole involves a weak bond and decomposes easily by a unimolecular reaction even at moderate temperatures. The addition of oxygen has very little influence under these conditions. Note that the oxygen consumption starts above 900 K, at a temperature for which anisole conversion is close to complete.

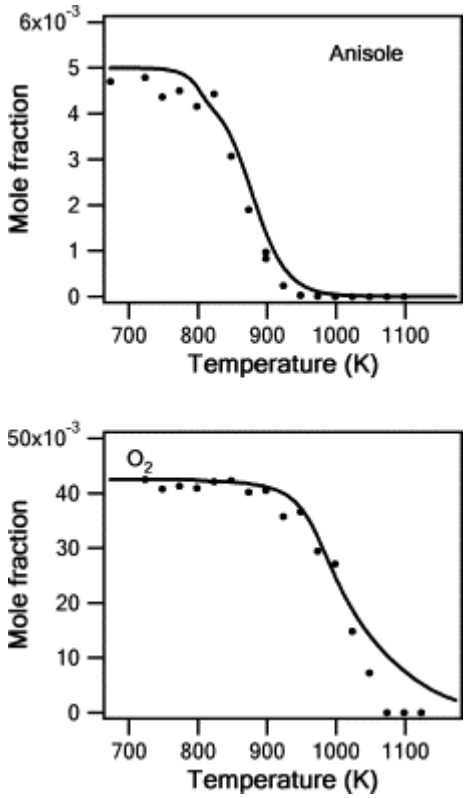

Figure 8: Evolution of the mole fraction of the reactants during the stoichiometric oxidation of anisole at residence time 2 s and pressure 800 Torr. Points refer to experiments and lines to modeling.

In contrast to pyrolysis results, it appears that the addition of oxygen does not significantly affect the nature of the main products at low temperatures, but leads to the combustion products (CO and CO_2) at high temperatures, instead of producing aromatics and soot. The mole fraction profiles of the light products are displayed in Figure 9. The only new C_1-C_2 products are carbon dioxide and acetaldehyde. CO and H_2 mole fractions reach a maximum around 1000 K and are completely converted to CO_2 and water at 1100 K. The amount of C_2 compounds is lower than in pyrolysis. Ethylene remains the major one (800 ppm at the peak, close to the maximum amount of methane), followed by ethane (300 ppm) and acetylene (250 ppm). Acetaldehyde is abundant around 950 K (150 ppm). The nonaromatic heavier compounds are presented in Figure 10. Acrolein (75 ppm around 950 K) and 1-butene (12 ppm at 925 K) have been quantified in oxidation, while propane was not detected anymore. We can observe that the higher reactivity induced by the presence of oxygen in the mixture above 900 K leads to larger amounts of C_3 and C_4 compounds in comparison with pyrolysis. The peak of propene is now close to 45 ppm, while 1,3-butadiene and vinylacetylene maximum fractions are respectively three times and twice those obtained in pyrolysis. This can be explained by the greater decomposition of the aromatic intermediates allowed by their reactions with oxygenated radicals. Conversely, 1,3-cyclopentadiene and 5-methyl,1,3-cyclopentadiene amounts have dropped off.

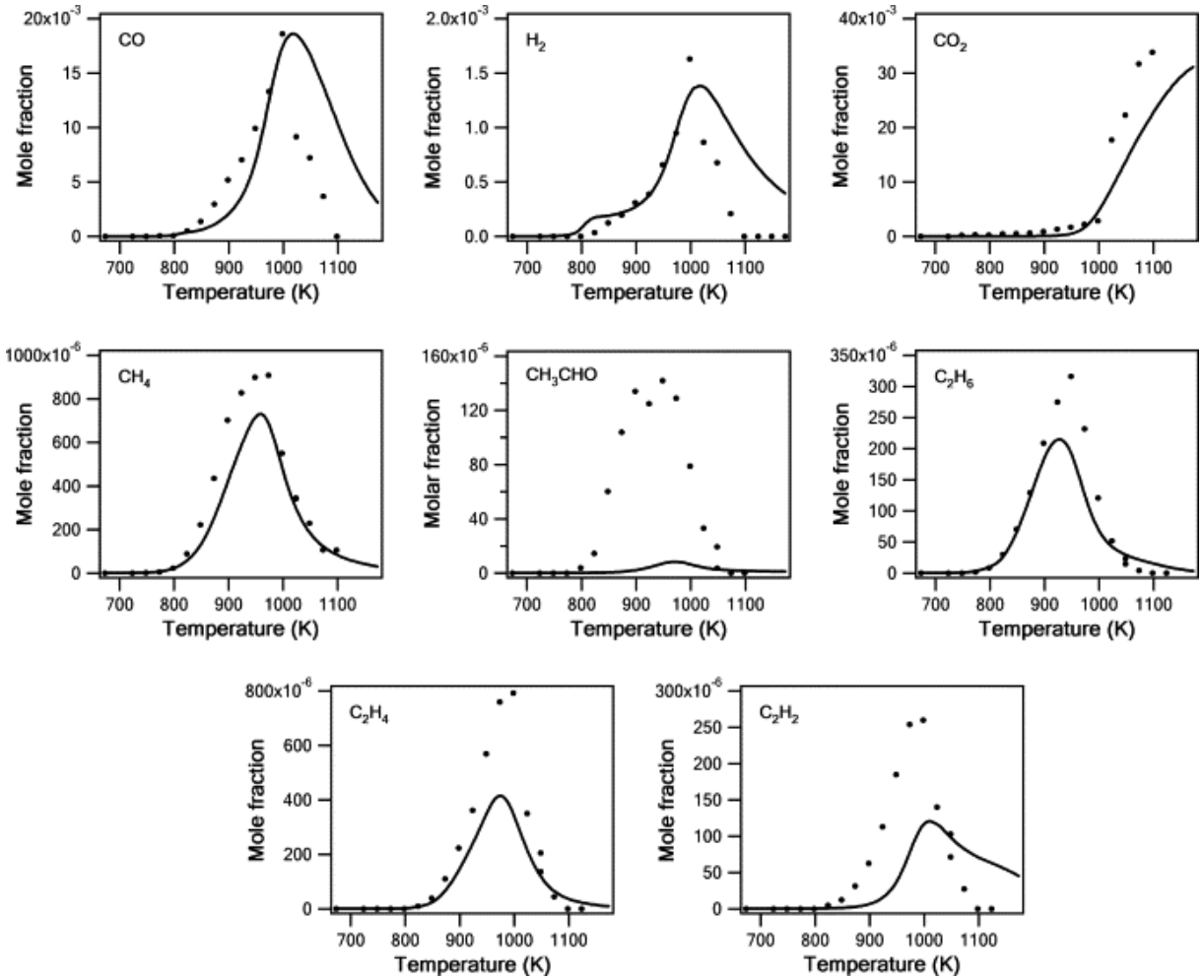

Figure 9: Evolution of the mole fraction of light products during the stoichiometric oxidation of anisole at residence time 2 s and pressure 800 Torr. Points refer to experiments and lines to modeling.

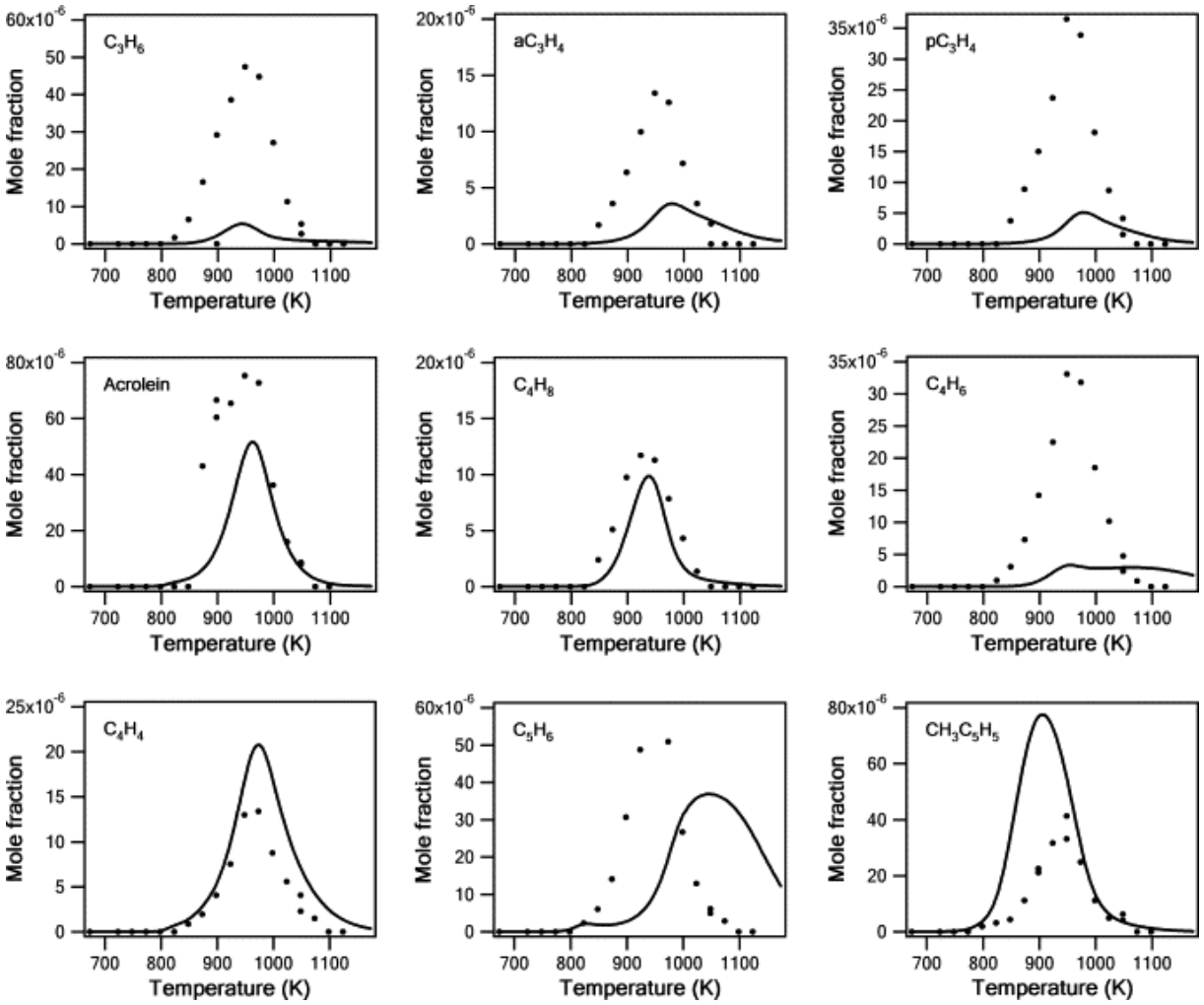

Figure 10: Evolution of the mole fraction of nonaromatic C_3-C_6 products during the stoichiometric oxidation of anisole at residence time 2 s and pressure 800 Torr. Points refer to experiments and lines to modeling.

Figure 11 displays the profiles of aromatic products. The same products as in pyrolysis have been quantified, except m-guaiacol and hydroxybenzaldehyde, which were detected only in oxidation, and o- and p-xylenes, ethylbenzene, and acenaphthylene, which were not detected in oxidation. Phenol is the major aromatic product (around 1300 ppm at 900 K), while the maximum amounts of cresols and benzofuran decrease to 310 ppm and 150 ppm around 900–950 K, respectively. The amount of benzaldehyde, which is produced at low temperatures, is similar to that obtained in pyrolysis. Among the nonoxygenated aromatics, the most abundant product is benzene (370 ppm). In comparison with pyrolysis, the amount of naphthalene drops off dramatically to 20 ppm, which is consistent with the decrease in the amount of precursors such as C_5H_6. Traces of 2,3-dihydrobenzofuran and xanthone were identified but not quantified. Among the reaction products, the larger selectivity was obtained for carbon monoxide, phenol, carbon dioxide, methane, benzaldehyde, cresol, and hydrogen at 873 K. At 1023 K, anisole is mainly converted to carbon monoxide, phenol, and carbon dioxide. The maximum mole fraction of naphthalene is reached at about 1000 K and this compound is then completely converted under oxidative conditions, whereas its maximum was obtained at 1150 K under pyrolysis conditions without any further decrease in its profile.

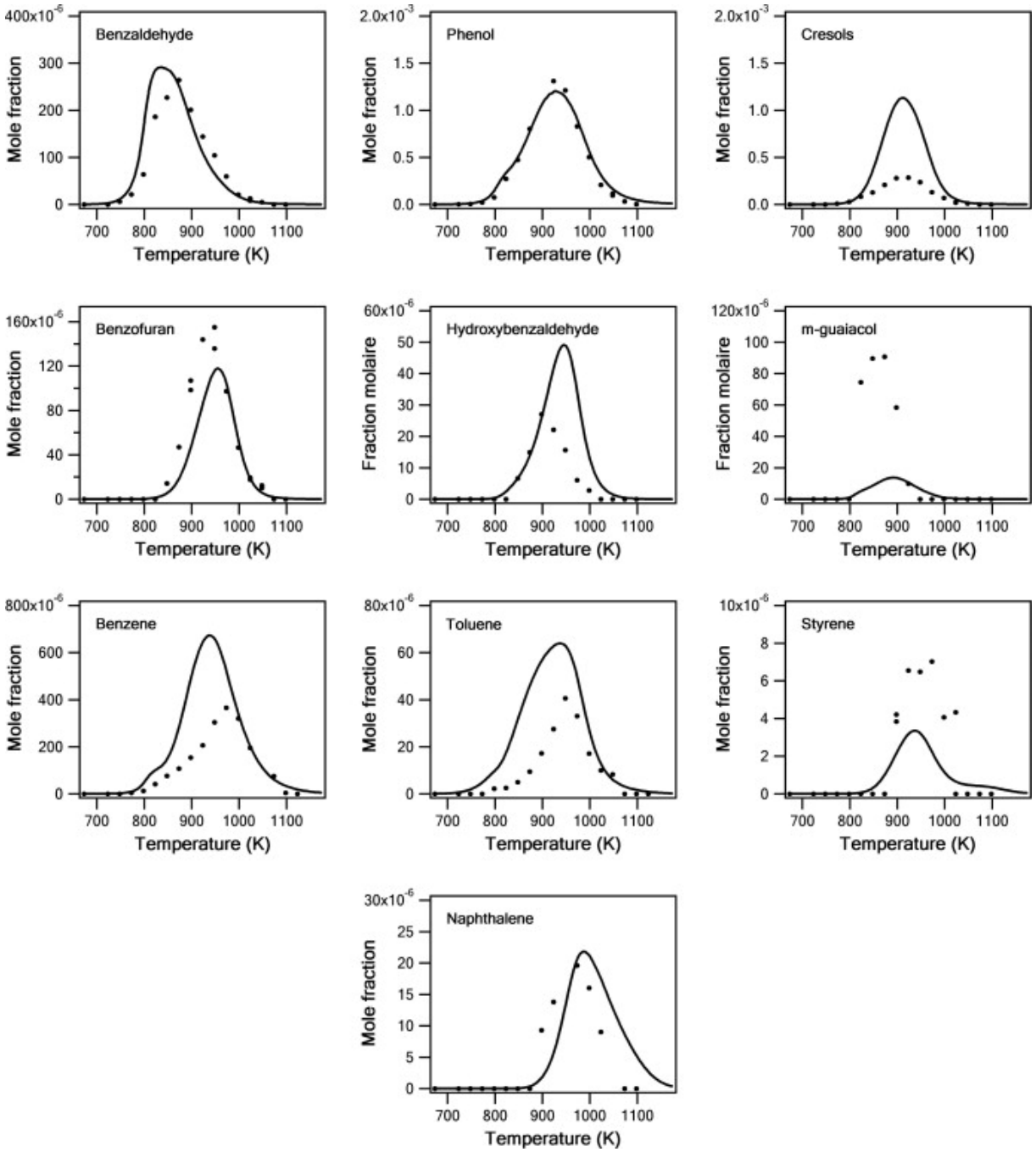

Figure 11: Evolution of the mole fraction of aromatic products during the stoichiometric oxidation of anisole at residence time 2 s and pressure 800 Torr. Points refer to experiments and lines to modeling.

4.2. Comparison between experimental data and simulations

The detailed model developed in this study aims at predicting the conversion of anisole and the formation of the main products on a large range of residence times and thermal conditions. The predictions using the model were compared to our experimental data (Figures 3, 4, 5 and 6 in pyrolysis, Figures 8, 9, 10 and 11 in oxidation). To extend the validity of the model, results obtained in the Princeton flow reactor by Pecullan et al. [20] were also simulated. In both thermal decomposition and oxidation, the model predicts the anisole reactivity perfectly (Figures 3 and 8). The model simulates well the complete conversion of the reactant achieved at 950 K under both conditions and the profiles of the primary products. At higher temperatures, some discrepancies between simulations and experiments increase since the reaction is not that of anisole any more, but that of a very complex mixture of phenolic, aromatic, or furanic products. The amounts of most minor products are, however, estimated within a factor of 2. Note that the model uses as a reaction base a mechanism for light aromatics (benzene, toluene, ethylbenzene) validated under various condition of combustion [29], [32] and [59]. Consequently, arbitrary adjustments of reactions in this submechanism have been avoided since they would yield little further information, but might change results for aromatic combustion drastically.

In pyrolysis, the behavior of the light products is well reproduced (Figure 4). Hydrogen and methane, which are produced by H-atom abstractions by H-atoms and methyl radicals, respectively, are correctly simulated at the lowest temperature, showing that the rate constants of the H-atom abstractions on anisole are correctly estimated. When the temperature increases, hydrogen is slightly overpredicted and methane underpredicted, reflecting the fact that H-atom abstractions on anisole become a minor channel in the formation of these light molecules above 830 K, conversely to H-atom abstraction on cresols, benzaldehyde, phenol, and 5-methyl,1,3-cyclopentadiene. Many of these latter rate constants are just estimates by means of structure–reactivity relationships. Ethylene is a little overestimated, while ethane is slightly underestimated, but the order of magnitude is correct. A major source of ethylene is the reaction between methyl radicals and $HOC_6H_4CH_2$ radicals that derive from cresol molecules, yielding ethylene and phenol. The product distribution and the rate constant of this reaction contained in the xylene submechanism [34] are estimated and uncertain. The amounts of C_3 and C_4 light products are simulated at least within a factor of 2 but the profile shapes fit the experimental data well (Figure 5). Vinylacetylene is the only one that is strongly underestimated. However, these intermediates are formed in small quantities, mostly above 900 K, and do not correspond to primary products of anisole decomposition but rather to products from other reactions, such as reactions of C_2 and the decomposition of aromatic rings. This induces larger uncertainties in their modeling. 1,3-Cyclopentadiene, which is produced by the decomposition of phenoxy radicals, and 5-methyl,1,3-cyclopentadiene, obtained from the combination of a methyl and a cyclopentadienyl radical, are also a little underestimated.

The simulation of aromatic products presented in Figure 6 is almost satisfactory. Considering the well-known experimental difficulties encountered in the quantification of phenols [18] and [60], the oxygenated aromatics, which are formed during the early stage of anisole decomposition, are rather well reproduced, at least below 950 K. The mole fraction of phenol is, however, underpredicted, while that of cresols is overpredicted around 900 K. The formation of these species is competing through the fate of the phenoxy radical. We have used the values proposed by Pecullan et al. for the phenoxy + methyl radical multichannel reaction [20]. These rate constants theoretically evaluated are the only ones available in the literature, but lead to these slight discrepancies. The underprediction of benzofuran at low temperatures suggests, however, the lack of a route of formation for this compound. Among the cyclic hydrocarbons, benzene is correctly predicted at the lowest temperatures, but the model does not reproduce the experimental results above 900 K very well: its formation is first overpredicted and its amount decreases dramatically above 1000 K, unlike the experiments. Conversely, naphthalene, which is formed mainly from the combination of two

cyclopentadienyl radicals, is overvalued by a factor of 3 above 1000 K. Benzene is mostly formed in our model by reactions of 5-methyl,1,3-cyclopentadiene. 5-Methyl,1,3-cyclopentadiene comes at the lowest temperatures from the reaction of phenoxy radicals with CH3 proposed by Pecullan et al. [20] and, when the temperature increases, from the combination of methyl and cyclopentadienyl radicals. The discrepancy in the simulation of benzene and naphthalene at high temperature is linked to the modeling of reactions of 1,3-cyclopentadiene and cyclopentadienyl radicals, which are especially tricky in pyrolysis in a complex mixture of unsaturated hydrocarbons and radicals. All the possible reactions are still not completely understood and are under discussion in the literature [50], [61], [62], [63] and [64]. Especially, we have tried to describe more accurately the formation of naphthalene, including recent theoretical studies [62] and [63]. However, the simulated results changed only marginally and the lack of information about the bimolecular reactions of the new intermediates added more uncertainties. Eventually, the reaction of two C_5H_5 radicals yielding naphthalene and two H-atoms was preferred, with the rate constant proposed by Melius et al. [65]. Note, however, that the sum of the simulated mole fractions of benzene and naphthalene fits the experimental value well. Even if the formation of some PAHs has been taken into account in the model [35], the lack of soot formation may also contribute to an undervalued consumption of naphthalene.

Despite the small amount of xylenes (below 15 ppm), the model overpredicts the quantity of these species by a factor of 1.5 (o-xylene) and 3 (p-xylene). For ethylbenzene and styrene, the model overvalues the quantities a little compared to the experimental results. Beyond the compounds which have been quantified experimentally, the model predicts also some polyaromatic compounds such as pyrene, indene, and phenanthrene, thanks to the addition of the submechanism from Slavinskaya et al. [35]. Their simulated profiles are presented in Figure S2 in the Supplemental material. Pyrene, often used in models as the precursor for soot inception, reaches 400 ppm at 1100 K.

In the presence of oxygen, the conversion of the reactants is presented in Figure 8. The model prediction follows the experimental profiles perfectly. The major light products (Figures 9 and 10), such as CO, CO_2, and methane, are very well represented by the model. The other C_1-C_2 species (Figure 9), which are produced in small quantities (20–800 ppm), are well reproduced, except in the case of acetaldehyde, an oxidation product of the small unsaturated species such as propene. This underprediction can be related to the underprediction of propene or 1,3-butadiene (Figure 10). As in pyrolysis, these latter molecules are produced by the decomposition of the aromatic rings, in which many uncertainties remain in the C_2-C_4 product distribution, especially at the low temperatures investigated here. 1,3-Cyclopentadiene has a simulated profile slightly shifted toward the higher temperatures. Note that 1,3-cyclopentadiene is a very reactive species, which is in a quasi-equilibrium with resonance-stabilized cyclopentadienyl radicals. A small uncertainty in the production or consumption fluxes leads to a large variation of its mole fraction. At low anisole conversion, i.e., without the strong influence of secondary reactions, 1,3-cyclopentadiene is rather well reproduced (see Figure 10). Heavy products displayed in Figure 11 are very well simulated. The simulated profiles of benzaldehyde, benzofuran, benzene, toluene, and naphthalene are well estimated. This means that the most important channels of formation and consumption of these compounds are well handled by the mechanism. Only cresols are overestimated by a factor of 2. As written above, the rate constants theoretically determined by Pecullan et al. [20] for the reactions of phenoxy and methyl radicals lead to an overestimation of this channel. Hydroxybenzaldehyde is produced by the oxidation of the methyl group of cresols and is then slightly overpredicted at temperatures above 900 K. Among the phenolic species, m-guaiacol is the only one to be undervalued by the model, indicating that a formation pathway may be missing. m-Guaiacol comes in modeling from the combination of methyl and HOC_6H_4O radicals, this latter radical being produced by a H-atom abstraction and an oxidation reaction on the aromatic cycle of phenol. The discrepancies between experiments and simulations found in pyrolysis for hydrocarbons above 1000 K do not

appear in oxidation. Since the complex molecular growth yielding soot precursors competes now with some fast oxidation reactions with O-atoms, OH radicals, or O_2 molecules, which oxidize aromatic molecules and radicals into smaller species. As stated above, the distribution of the products of these latter reactions is more uncertain, leading to a less accurate modeling of C_3-C_4 molecules. The simulations also show a strong decrease in the xylene formation (Figure S3 in the Supplemental material), below 0.1 ppm. This explains why these species were not found experimentally anymore. The heavy polycyclic molecules are also present in oxidation; however, the predicted quantities of phenanthrene and pyrene are below 1 ppm.

In order to validate the primary model of decomposition of anisole, the experimental results obtained by Pecullan et al. [20] at atmospheric pressure near 1000 K have been also simulated. A short residence time of about 100 ms made it possible to form principally the primary products from anisole decomposition. Figure 12 displays experimental data and simulations in pyrolysis as a function of residence time for an inlet mole fraction of 1077 ppm of anisole and a temperature of 1003 K. A shift of 7 ms was done in the simulation in order to take into account the uncertainty of the zero point in the flow reactor. The model reproduces perfectly the anisole consumption and the formation of CO, 1,3-cyclopentadiene, and benzene. More differences are obtained with cresols and phenol, but these products are more difficult to quantify experimentally [60], and the uncertainty in the rate constant of the reaction producing cresols was discussed above. Other validations against these data, especially in oxidation, are presented in the Supplementary material (Figure S5).

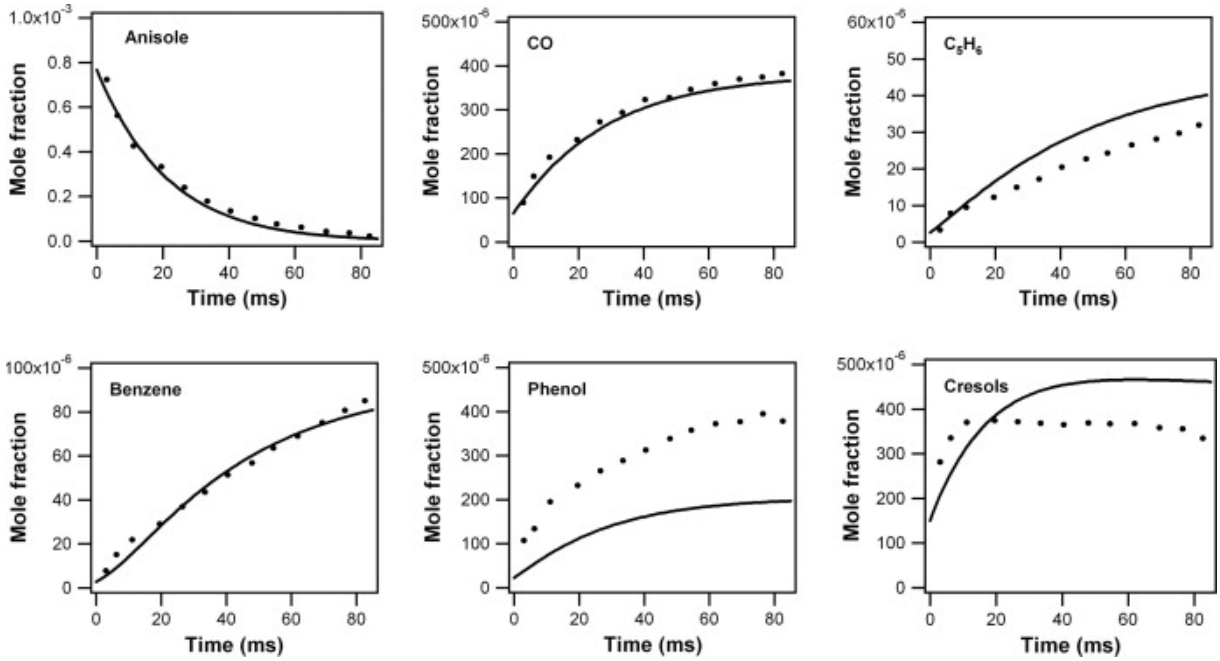

Figure 12: Mole fraction profiles of reactant and selected products during the pyrolysis of anisole in the Princeton flow reactor [18]. $X_{anisole}$ = 1077 ppm, T = 1003 K, P = 1 atm. Points refer to experiments and lines to the present modeling.

4.3. Analysis and discussion

The reaction pathways involved in the conversion of anisole are illustrated in Figure 13 at 800 K and Figure 14 at 1000 K, under the conditions of the jet-stirred experiments. At 800 K, the simulated conversion is 12% and anisole reacts mainly by the unimolecular bond breaking, yielding methyl and phenoxy radicals (42% of the total anisole consumption). At this low temperature, the decomposition of the resonance-stabilized phenoxy radicals to CO and cyclopentadienyl radicals does not occur. The phenoxy radicals react rather by H-atom abstraction on anisole or primary products to produce

phenol or with CH_3 to produce cresols and to a lesser extent CO and 5-methyl,1,3-cyclopentadiene. Phenol and cresols come almost completely from phenoxy radicals. Anisole reacts also by H-atom abstraction by H-atom, methyl, phenyl, and phenoxy radicals (39% of the total anisole consumption). These reactions yield $C_6H_5OCH_2$ radicals, which isomerize entirely to $C_6H_5CH_2O$. This latter decomposes mainly to benzaldehyde. Minor routes of consumption of anisole are ipso-additions of H-atoms yielding benzene (14%) and of methyl radicals yielding toluene (5%). When the temperature increases, the bimolecular reactions of anisole does not compete any more with the bond breaking and becomes negligible. At 1000 K, the conversion is almost complete and 99.9% of anisole is converted into phenoxy and methyl radicals. Phenoxy radicals react still with methyl radicals to produce cresols and by H-atom abstraction or by combination with H-atoms to produce phenol, but another important reaction channel is now the decomposition to CO and C_5H_5 radical through a bicyclic intermediate. C_5H_5 recombines mostly with itself to form naphthalene, with CH_3 to produce 5-methyl,1,3-cyclopentadiene, and with H-atoms leading to 1,3-cyclopentadiene. The reaction of phenoxy radicals with o-cresol to form benzofuran is a very minor channel.

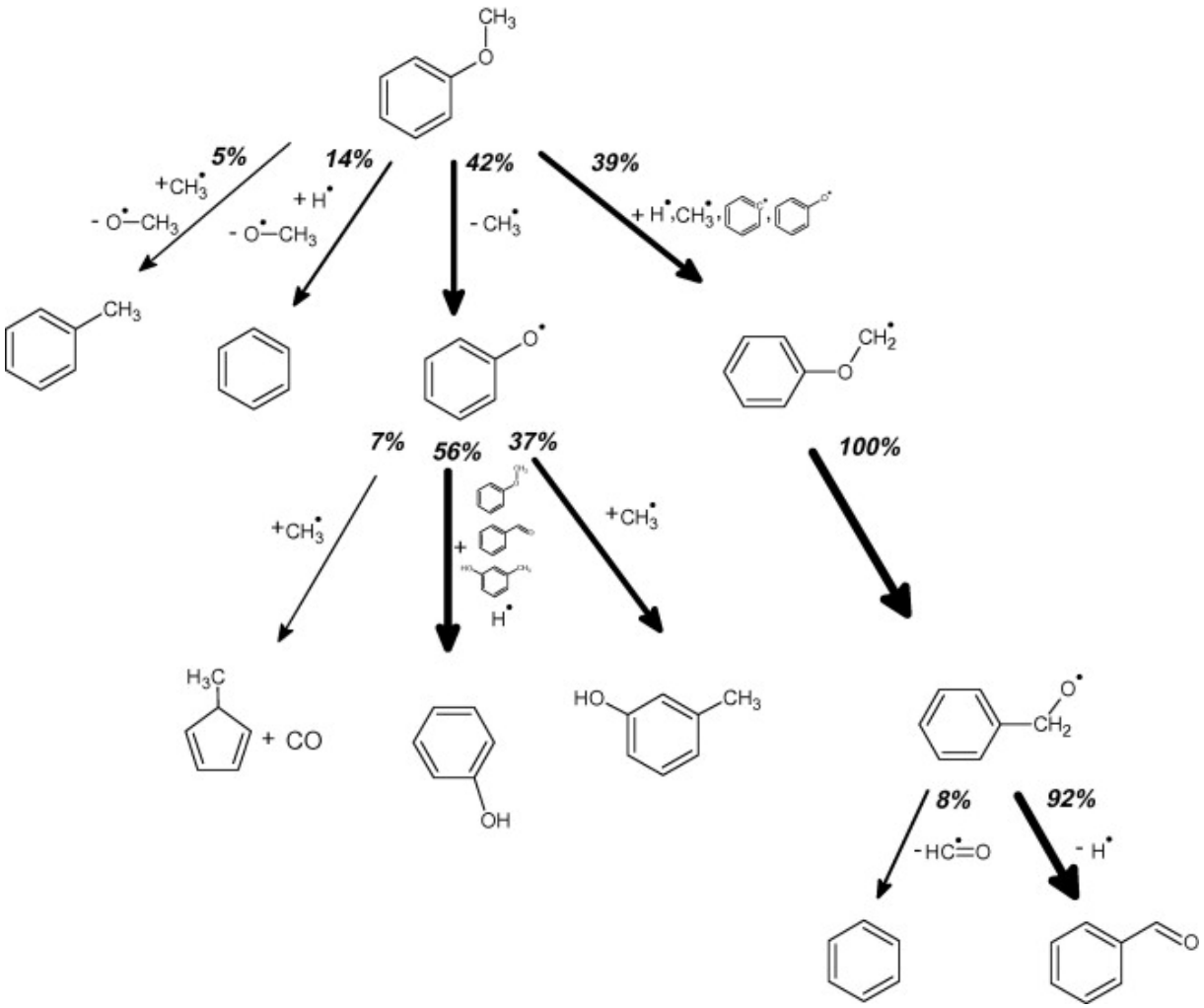

Figure 13: Reaction flux analysis for anisole pyrolysis at 800 K, 800 Torr, residence time of 2 s corresponding to 12% anisole conversion. Reaction fluxes (numbers associated with arrows) are relative to the consumption of a given species.

Concerning the oxidation conditions, the reaction routes are almost the same as in pyrolysis. Reaction flow schemes in oxidation are presented in the Supplementary material (Figures S6 and S7). At low temperatures, unimolecular decomposition decreases to 32% and the proportion of the H-atom abstractions increases to 60% of the consumption of anisole. OH radicals and O-atoms

enhance this latter channel. The fate of the produced radicals is not influenced by the presence of oxygen. At 1000 K, the role of metatheses is very minor, but their flow grows to 7%, with OH radicals. The main reaction channel remains the anisole decomposition by breaking of the O-CH_3 bond. The major change in the fate of phenoxy radicals is the decrease in the production of cresols by reaction with CH_3 radicals and the enhancement of the formation of phenol by reaction with HO_2 radicals. The similarity of the reaction channels in pyrolysis and in oxidation, caused by the weakness of the O-CH_3 bond, explains why the conversion of the fragile anisole molecule is not influenced by the addition of oxygen under our conditions.

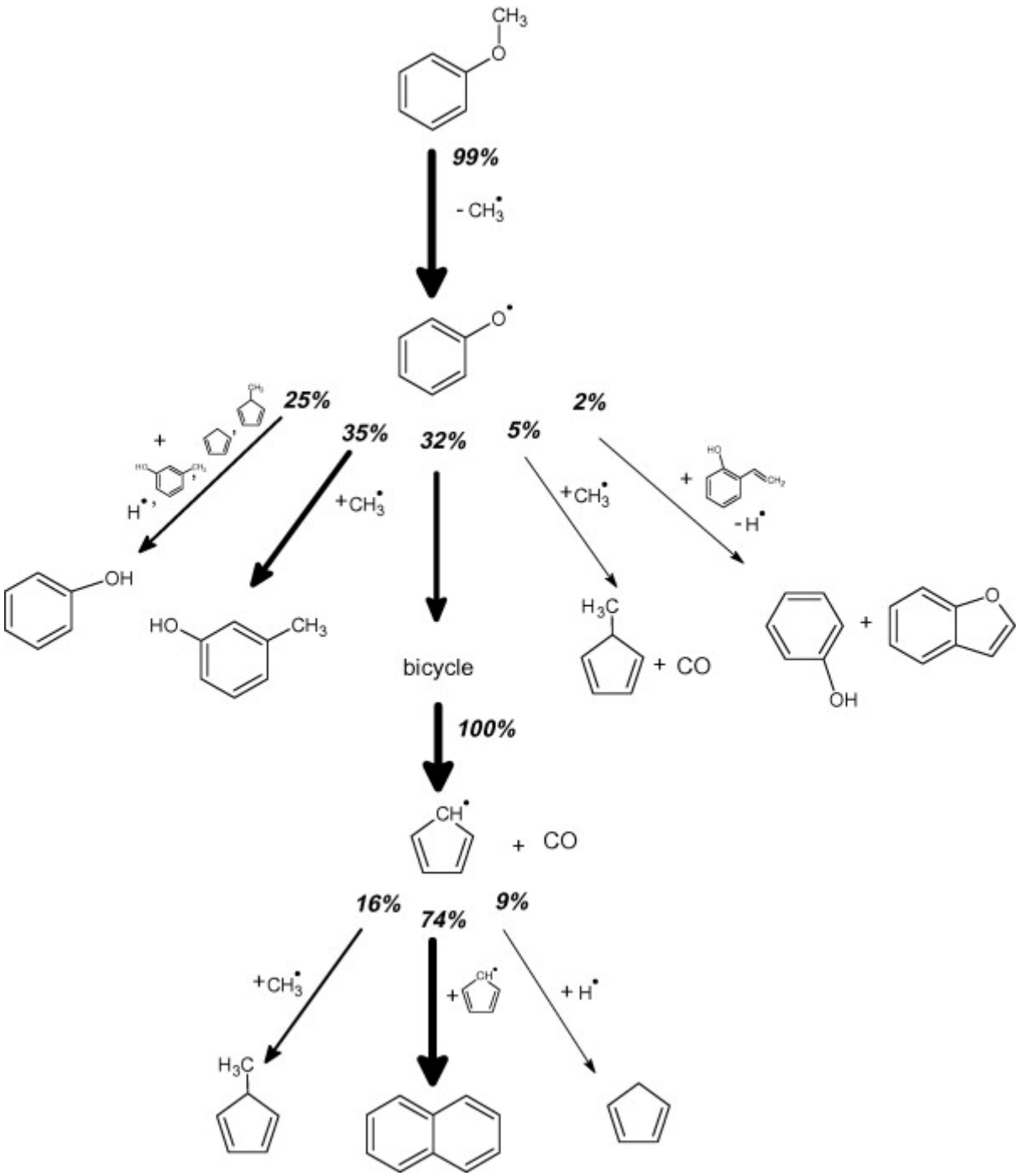

Figure 14: Reaction flux analysis for anisole pyrolysis. Conditions: 1000 K, 800 Torr, residence time of 2 s corresponding to 99.9% anisole conversion. Reaction fluxes (numbers associated with arrows) are relative to the consumption of a given species.

Sensitivity analyses performed in pyrolysis at 800 and 1000 K confirm the relative simplicity of the initial channels of anisole reaction (Figure 15; coefficients at 1000 K have been divided by 10). At 800 K, the promoting reactions for anisole conversion are the unimolecular initiation and the metatheses with H-atom, methyl, and phenoxy radicals. The only noticeable inhibiting termination is the combination of phenoxy radicals with H-atoms, producing phenol. At high temperatures, the unimolecular initiation becomes by far the most sensitive step. Since the radical bimolecular reactions are then negligible in anisole consumption, no inhibiting process really appears. Very similar results were obtained in oxidation, which explain the similar reactivity of anisole in pyrolysis and oxidation whatever the equivalence ratio [20].

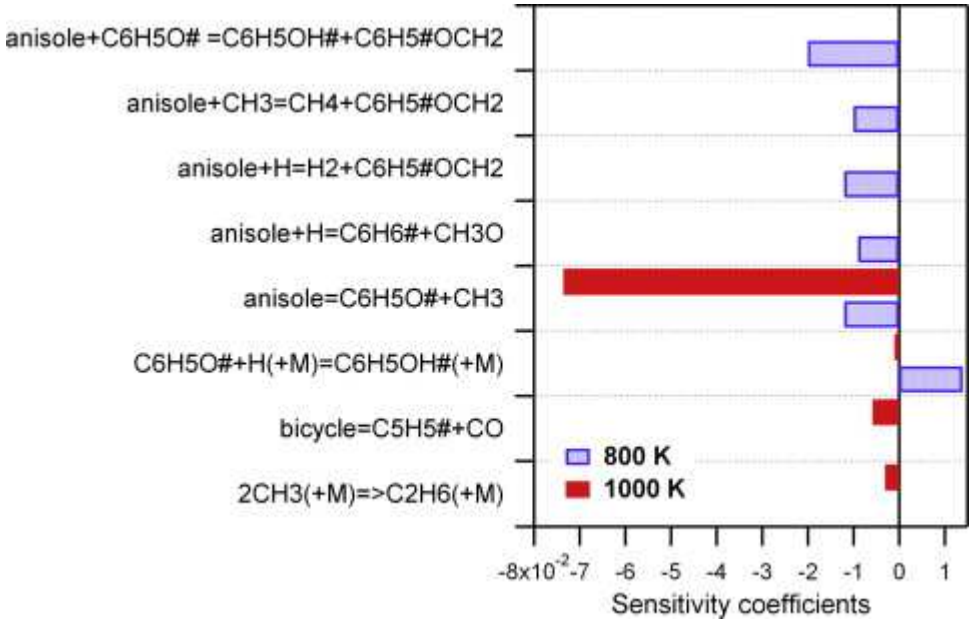

Figure 15: Sensitive reactions in the consumption of anisole in pyrolysis at 800 and 1000 K. Coefficients at 1000 K have been divided by 10 for presentation.

One of the main concerns in biomass combustion or gasification processes is the formation of tertiary tars, PAHs, and ultimately soot. During the decomposition of the lignin, large amounts of methoxyphenols are released. Anisole is a simplified surrogate of many methoxy-phenols formed during lignin pyrolysis [66]. More complex methoxyphenols such as guaiacol involve the same methoxy group and should react in the same way. Anisole decomposes to phenoxy radicals, which leads to large amounts of cyclopentadienyl radicals. At 1000 K, C_5H_5 produces mainly naphthalene in pyrolysis. In oxidation, this PAH is still formed by the combination of two C_5H_5 radicals, but its formation is in competition with the oxidation of the radicals, which reaches 75% of C_5H_5 consumption, as shown in the flow analysis of cyclopentadienyl radicals presented in the Supplemental material (Figure S8). Figure 16 displays the sensitive reactions to the formation of naphthalene at 1000 K. In pyrolysis, the most promoting reaction is the decomposition of the bicyclic intermediate (bicycle in Figure 16) formed in the phenoxy radicals to CO + C_5H_5 pathway. This reaction involves a high activation energy and is the primary source of C_5H_5 radicals. The formation of the bicycle from phenoxy radicals is then also promoted. The combination of two methyl radicals to form ethane also promotes naphthalene formation by removing CH_3 from the mixture, since this latter radical can also combine with C_5H_5 to yield 5-methyl,1,3-cyclopentadiene. The inhibiting reactions are mainly the combinations of phenoxy radicals with H-atoms and methyl radicals, which compete with the decomposition to C_5H_5, and that of C_5H_5 and methyl radicals. In oxidation, the limiting step in the formation of naphthalene is no longer the formation of C_5H_5 radical from phenoxy radicals, but the combination of C_5H_5, which competes with its oxidation by some reactions with O_2 and HO_2. The reactions of phenol with O-atoms and OH radicals to produce hydroxyphenoxy and

hydroxyphenyl radicals also inhibit the formation of naphthalene by competition with the reactions of formation of the phenoxy radical, a precursor of C_5H_5.

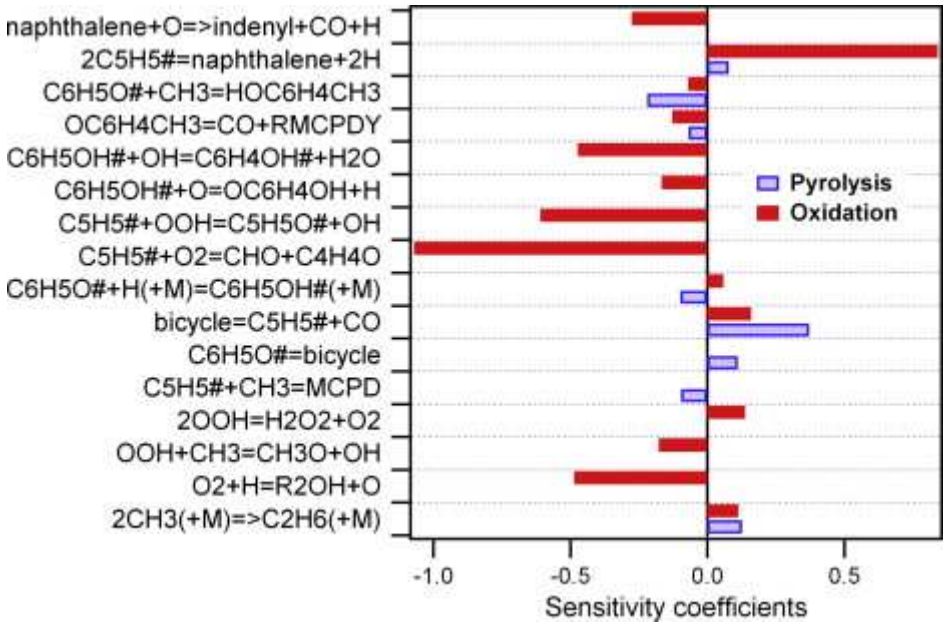

Figure 16: Sensitive reactions in the production of naphthalene at 1000 K during pyrolysis and oxidation of anisole.

5. Conclusions

In biomass combustion and gasification reactors, the first steps of reaction are a thermal decomposition, which generates hundreds of primary tars from cellulose, hemicelluloses, and lignin. These species are further converted in the gas phase in what is called tar maturation, i.e., their evolution toward species with lower O/C and H/C ratios. Lignin pyrolysis produces methoxyphenols, including heavy oligomers. Using anisole as a surrogate for lignin primary tars, its thermal decomposition and its oxidation under stoichiometric conditions at moderate temperatures have been studied. It was found that the decomposition of such a fragile molecule occurs mainly by the breaking of the methoxy O-C bond, producing large amounts of phenoxy radicals. This leads to some observations.

• The decomposition of anisole, and thereafter that of methoxyphenols, is a first-order reaction that occurs easily even at moderate temperature, without any influence of the addition of oxygen.

• The main primary products are phenol and phenolic molecules (secondary tars).

• Further reactions of the primary products lead mainly to cyclopentadienyl radicals and 1,3-cyclopentadiene, which are well-known PAH and soot precursors.

• An early formation of first aromatic rings and of naphthalene occurs, which does not involve the usual mechanisms of PAH formation in combustion based on C_2 or C_3 species [67].

The HACA mechanism looks like a minor route for PAH formation below 1000 K in biomass gasification or mild combustion reactors. Indeed, PAHs are already formed from 900 K under pyrolysis [68] or oxidation [69] conditions and CH_4 and C_2 compounds are poorly converted under slightly oxidizing conditions [70]. PAHs in biomass gasification or mild combustion reactors would be mainly formed (from 900 to 1100 K) from phenoxy radicals, producing cyclopentadienyl radicals and further PAHs and soot. This finding, derived from this study on anisole, needs to be confirmed for a broader range of temperatures, with other model compounds (such as furans from carbohydrates), and on real biomass gas.

Acknowledgments

This work was partially supported by the Energy program of CNRS through the project “CRAKIN” and the French ANR through the project “GAMECO” (coordinated by EDF).

References

[1] W. Klose, M. Wölki, Fuel, 84 (2005), pp. 885–892
[2] C. Di Blasi, Prog. Energy Combust. Sci., 34 (2008), pp. 47–90
[3] A.V. Bridgwater, Fuel, 74 (1995), pp. 631–653
[4] T.A. Milne, R.J. Evans, N. Abatzoglou, Biomass Gasifier “tars”: Their Nature, Formation, and Conversion, National Renewable Energy Laboratory (NREL), Golden, CO, n.d.
[5] R.J. Evans, T.A. Milne, Energy Fuels, 1 (1987), pp. 123–137
[6] A. Dufour, P. Girods, E. Masson, S. Normand, Y. Rogaume, A. Zoulalian, J. Chromatogr. A, 1164 (2007), pp. 240–247
[7] J. Corella, A. Orío, J.-M. Toledo, Energy Fuels, 13 (1999), pp. 702–709
[8] A. Donnot, P. Magne, X. Deglise, J. Anal. Appl. Pyrol., 22 (1991), pp. 47–59
[9] M.D. Hays, B. Gullett, C. King, J. Robinson, W. Preston, A. Touati, Energy Fuels, 25 (2011), pp. 5632–5638
[10] A. Dufour, J. Weng, L. Jia, X. Tang, B. Sirjean, R. Fournet et al., RSC Adv., 3 (2013), pp. 4786–4792
[11] M.W. Jarvis, T.J. Haas, B.S. Donohoe, J.W. Daily, K.R. Gaston, W.J. Frederick et al., Energy Fuels, 25 (2011), pp. 324–336
[12] E.M. Fitzpatrick, J.M. Jones, M. Pourkashanian, A.B. Ross, A. Williams, K.D. Bartle, Energy Fuels, 22 (2008), pp. 3771–3778
[13] E.-J. Shin, M.R. Nimlos, R.J. Evans, Fuel, 80 (2001), pp. 1681–1687
[14] A.K. Vasiliou, J.H. Kim, T.K. Ormond, K.M. Piech, K.N. Urness, A.M. Scheer et al., J. Chem. Phys., 139 (2013)
[15] M. Mulcahy, B. Tucker, D. Williams, J. Wilmshurst, Aust. J. Chem., 20 (1967), pp. 1155–1171
[16] R.H. Schlosberg, P.F. Szajowski, G.D. Dupre, J.A. Danik, A. Kurs, T.R. Ashe et al., Fuel, 62 (1983), pp. 690–694
[17] C.-Y. Lin, M.C. Lin, J. Phys. Chem., 90 (1986), pp. 425–431
[18] J.C. Mackie, K.R. Doolan, P.F. Nelson, J. Phys. Chem., 93 (1989), pp. 664–670
[19] I.W.C.E. Arends, R. Louw, P. Mulder, J. Phys. Chem., 97 (1993), pp. 7914–7925
[20] M. Pecullan, K. Brezinsky, I. Glassman, J. Phys. Chem. A, 101 (1997), pp. 3305–3316
[21] V.V. Platonov, V.A. Proskuryakov, S.V. Ryl’tsova, Y.N. Popova, Russ. J. Appl. Chem., 74 (2001), pp. 1047–1052
[22] A.V. Friderichsen, E.-J. Shin, R.J. Evans, M.R. Nimlos, D.C. Dayton, G.B. Ellison, Fuel, 80 (2001), pp. 1747–1755
[23] A.M. Scheer, C. Mukarakate, D.J. Robichaud, G.B. Ellison, M.R. Nimlos, J. Phys. Chem. A, 114 (2010), pp. 9043–9056
[24] A.M. Scheer, C. Mukarakate, D.J. Robichaud, M.R. Nimlos, G.B. Ellison, J. Phys. Chem. A, 115 (2011), pp. 13381–13389
[25] E.B. Hemings, G. Bozzano, M. Dente, E. Ranzi, Chem. Eng. Trans., 24 (2011), pp. 61–66
[26] Y.R. Luo, Handbook of Bond Dissociation Energies in Organic Compounds, CRC Press, Boca Raton, FL (2003)
[27] C. Muller, V. Michel, G. Scacchi, G.M. Côme, J. Chim. Phys., 92 (1995), pp. 1154–1178
[28] M.H. Hakka, P.-A. Glaude, O. Herbinet, F. Battin-Leclerc, Combust. Flame, 156 (2009), pp. 2129–2144
[29] O. Herbinet, B. Husson, M. Ferrari, P.-A. Glaude, F. Battin-Leclerc, Proc. Combust. Inst., 34 (2013), pp. 297–305
[30] D. Matras, J. Villermaux, Chem. Eng. Sci., 28 (1973), pp. 129–137
[31] J. Tranchant, J.F. Gardais, P. Gorin, J. Serpinet, G. Untz, Manuel pratique de chromatographie en phase gazeuse, Masson, Paris, 1982.
[32] B. Husson, M. Ferrari, O. Herbinet, S.S. Ahmed, P.-A. Glaude, F. Battin-Leclerc, Proc. Combust. Inst., 34 (2013), pp. 325–333
[33] H.A. Gueniche, J. Biet, P.A. Glaude, R. Fournet, F. Battin-Leclerc, Fuel, 88 (2009), pp. 1388–1393
[34] F. Battin-Leclerc, R. Bounaceur, N. Belmekki, P.A. Glaude, Int. J. Chem. Kinet., 38 (2006), pp. 284–302
[35] N.A. Slavinskaya, U. Riedel, S.B. Dworkin, M.J. Thomson, Combust. Flame, 159 (2012), pp. 979–995
[36] R.J. Kee, F.M. Rupley, J.A. Miller, Sandia Laboratories Report, S 89-8009B, 1993.
[37] D. Baulch, C. Cobos, R. Cox, P. Frank, G. Hayman, T. Just et al., J. Phys. Chem. Ref. Data, 23 (1994), pp. 847–1033

[38] D.L. Allara, R. Shaw, J. Phys. Chem. Ref. Data, 9 (1980), pp. 523–560
[39] T. Ingham, R.W. Walker, R.E. Woolford, Symp. Int. Combust., 25 (1994), pp. 767–774
[40] T. Seta, M. Nakajima, A. Miyoshi, J. Phys. Chem. A, 110 (2006), pp. 5081–5090
[41] S. Touchard, F. Buda, G. Dayma, P.A. Glaude, R. Fournet, F. Battin-Leclerc, Int. J. Chem. Kinet., 37 (2005), pp. 451–463
[42] A.M. Dean, J.W. Bozzelli, Combustion chemistry of nitrogen, W.C. Gardiner Jr. (Ed.), Gas-Phase Combustion Chemistry, Springer, New York (2000), pp. 125–341
[43] J.T. Moss, A.M. Berkowitz, M.A. Oehlschlaeger, J. Biet, V. Warth, P.-A. Glaude et al., J. Phys. Chem. A, 112 (2008), pp. 10843–10855
[44] F. Buda, R. Bounaceur, V. Warth, P. Glaude, R. Fournet, F. Battin-Leclerc, Combust. Flame, 142 (2005), pp. 170–186
[45] W. Tsang, J. Phys. Chem. Ref. Data, 20 (1991), pp. 221–273
[46] J. Park, L.M. Wang, M.C. Lin, Int. J. Chem. Kinet., 36 (2004), pp. 49–56
[47] M. Mulcahy, D. Williams, Aust. J. Chem., 18 (1965), pp. 20–38
[48] G. da Silva, J.W. Bozzelli, J. Phys. Chem. A, 113 (2009), pp. 6979–6986
[49] Y.Z. He, W.G. Mallard, W. Tsang, J. Phys. Chem., 92 (1988), pp. 2196–2201
[50] B. Sirjean, R. Fournet, P.-A. Glaude, F. Battin-Leclerc, W. Wang, M.A. Oehlschlaeger, J. Phys. Chem. A, 117 (2013), pp. 1371–1392
[51] Z.F. Xu, M.C. Lin, J. Phys. Chem. A, 110 (2006), pp. 1672–1677
[52] R.K. Robinson, R.P. Lindstedt, Combust. Flame, 158 (2011), pp. 666–686
[53] X. Zhong, J.W. Bozzelli, J. Phys. Chem. A, 102 (1998), pp. 3537–3555
[54] G.-J. Nam, W. Xia, J. Park, M.C. Lin, J. Phys. Chem. A, 104 (2000), pp. 1233–1239
[55] N.M. Marinov, W.J. Pitz, C.K. Westbrook, A.M. Vincitore, M.J. Castaldi, S.M. Senkan et al., Combust. Flame, 114 (1998), pp. 192–213
[56] I.V. Tokmakov, M.C. Lin, J. Phys. Chem. A, 108 (2004), pp. 9697–9714
[57] A. Burcat, E. Goos, B. Ruscic, Ideal Gas Thermochemical Database with updates from Active Thermochemical Tables, 2013.
[58] B. Sirjean, E. Dames, D.A. Sheen, et al., A High-Temperature Chemical Kinetic Model of n-Alkane Oxidation, JetSurF Version 1.0, September 15, 2009. <http://melchior.usc.edu/JetSurF/Version1_0/Index.html>.
[59] R. Bounaceur, I. Da Costa, R. Fournet, F. Billaud, F. Battin-Leclerc, Int. J. Chem. Kinet., 37 (2005), pp. 25–49
[60] M. Pecullan, Pyrolysis and Oxidation Kinetics of Anisole and Phenol, Princeton University (1997)
[61] V.V. Kislov, A.M. Mebel, J. Phys. Chem. A, 112 (2008), pp. 700–716
[62] A.M. Mebel, V.V. Kislov, J. Phys. Chem. A, 113 (2009), pp. 9825–9833
[63] C. Cavallotti, D. Polino, Proc. Combust. Inst., 34 (2013), pp. 557–564
[64] A.M. Scheer, C. Mukarakate, D.J. Robichaud, G.B. Ellison, M.R. Nimlos, J. Phys. Chem. A, 114 (2010), pp. 9043–9056
[65] C.F. Melius, M.E. Colvin, N.M. Marinov, W.J. Pitz, S.M. Senkan, Symp. Int. Combust., 26 (1996), pp. 685–692
[66] R. Olcese, V. Carré, F. Aubriet, A. Dufour, Energy Fuels, 27 (2013), pp. 2135–2145
[67] H. Wang, M. Frenklach, Combust. Flame, 110 (1997), pp. 173–221
[68] A. Dufour, E. Masson, P. Girods, Y. Rogaume, A. Zoulalian, Energy Fuels, 25 (2011), pp. 4182–4189
[69] C.M. Kinoshita, Y. Wang, J. Zhou, J. Anal. Appl. Pyrol., 29 (1994), pp. 169–181
[70] A. Dufour, S. Valin, P. Castelli, S. Thiery, G. Boissonnet, A. Zoulalian, P.A. Glaude, Ind. Eng. Chem. Res., 48 (2009), pp. 6564–6572